Cell Reports
Physical Science

CellPress

Article

Perovskite Photovoltaics on Roll-To-Roll Coated Ultra-thin Glass as Flexible High-Efficiency Indoor Power Generators

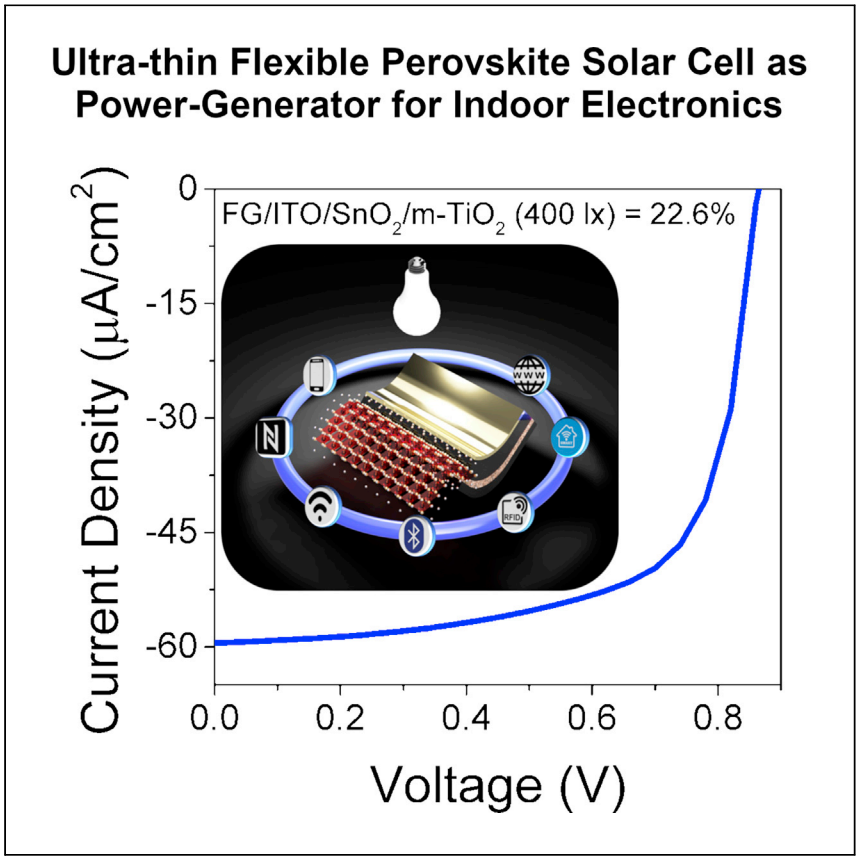

Indoor perovskite photovoltaics can help power the internet of things revolution, being highly efficient, low-cost, printable, and compatible with flexible substrates. Castro-Hermosa et al. develop flexible perovskite cells on roll-to-roll coated ultra-thin glass with excellent optoelectrical and mechanical properties, delivering efficiencies of 20.6%–22.6% under 200–400 lx LED illumination.

Sergio Castro-Hermosa, Giulia Lucarelli, Michiel Top, Matthias Fahland, John Fahlteich, Thomas M. Brown

thomas.brown@uniroma2.it

HIGHLIGHTS

Indoor efficiencies of 20.6%–22.6% on flexible glass under LED light

FG/PSCs outperform most current flexible indoor photovoltaics

Manufacturing process is compatible with low-cost roll-to-roll upscaling

PSCs are conformable, lightweight, and integrable with low-power devices

Castro-Hermosa et al., Cell Reports Physical Science *1*, 100045
May 20, 2020
https://doi.org/10.1016/j.xcrp.2020.100045

Please cite this article in press as: Castro-Hermosa et al., Perovskite Photovoltaics on Roll-To-Roll Coated Ultra-thin Glass as Flexible High-Efficiency Indoor Power Generators, Cell Reports Physical Science (2020), https://doi.org/10.1016/j.xcrp.2020.100045

Cell Reports
Physical Science

CellPress

Article

Perovskite Photovoltaics on Roll-To-Roll Coated Ultra-thin Glass as Flexible High-Efficiency Indoor Power Generators

Sergio Castro-Hermosa,[1,2,4] Giulia Lucarelli,[1,4] Michiel Top,[3] Matthias Fahland,[3] John Fahlteich,[3] and Thomas M. Brown[1,5,*]

SUMMARY

The internet of things revolution requires efficient, easy-to-integrate energy harvesting. Here, we report indoor power generation by flexible perovskite solar cells (PSCs) manufactured on roll-to-roll indium-doped tin oxide (ITO)-coated ultra-thin flexible glass (FG) substrates with notable transmittance (>80%), sheet resistance (13 Ω/square), and bendability, surpassing 1,600 bending procedures at 20.5-mm curvature. Optimized PSCs on FG incorporate a mesoporous scaffold over SnO_2 compact layers delivering efficiencies of 20.6% (16.7 $\mu W \cdot cm^{-2}$ power density) and 22.6% (35.0 $\mu W \cdot cm^{-2}$) under 200 and 400 lx LED illumination, respectively. These represent, to the best of our knowledge, the highest reported for any indoor flexible solar cell technology, surpassing by a 60%–90% margin the prior best-performing flexible PSCs. Specific powers (W/g) delivered by these lightweight cells are 40%–55% higher than their counterparts on polyethylene terephthalate (PET) films and an order of magnitude greater than those on rigid glass, highlighting the potential of flexible FG-PSCs as a key enabling technology for powering indoor electronics of the future.

INTRODUCTION

Perovskite solar cells (PSCs) are at the center of attention in the photovoltaic community, having reached certified power conversion efficiencies (PCEs) of 25.2% at the laboratory scale[1] when tested under standard test conditions (STCs), i.e., 1,000 W m^{-2} (1 sun) illumination, AM1.5G source spectrum, 25°C. In general, new-generation photovoltaics, including organic photovoltaics (OPVs),[2,3] dye-sensitized solar cells (DSSCs),[4,5] and PSCs[6–9] have delivered remarkable PCEs approaching 25%–30% at low illuminance typically found in most environments, such as homes and offices (i.e., 200–500 lx) and even greater than 30% at the more specific, limited environments of 1,000 lx (e.g., supermarkets), when tested under artificial light-emitting diode (LED) or fluorescent lamp illumination, surpassing all other PV technologies (i.e., silicon and thin-film-based cells) tested at low light levels. In addition to their outstanding performance in indoor environments, PSCs also bring the advantage of solution processability and low cost compared to first- and second-generation PV.[10–12] Indoor photovoltaics has the potential to enable the development of autonomous wireless sensors, low-power consumer electronics, and the internet of things ecosystem,[13] as it eliminates the need for battery usage and replacement, reduces the energy consumption in buildings, and allows independence from the electrical grid.[14] Billions of wireless sensors are expected to be installed over the coming decade.[14] The highest efficiencies reported for PSCs in indoor conditions

[1]CHOSE (Centre for Hybrid and Organic Solar Energy), Department of Electronic Engineering, University of Rome Tor Vergata, Via del Politecnico 1, 00133 Rome, Italy

[2]Hydro Engineering and Agricultural Development Research Group (GHIDA), Faculty of Engineering, Universidad Surcolombiana, Avenida Pastrana Borrero - Carrera 1, 410001 Neiva, Colombia

[3]Fraunhofer Institute for Organic Electronics, Electron Beam and Plasma Technology FEP, Winterbergstrasse 28, 01277 Dresden, Germany

[4]These authors contributed equally

[5]Lead Contact

*Correspondence: thomas.brown@uniroma2.it

https://doi.org/10.1016/j.xcrp.2020.100045

Please cite this article in press as: Castro-Hermosa et al., Perovskite Photovoltaics on Roll-To-Roll Coated Ultra-thin Glass as Flexible High-Efficiency Indoor Power Generators, Cell Reports Physical Science (2020), https://doi.org/10.1016/j.xcrp.2020.100045

have been achieved on rigid glass substrates. However, to successfully integrate solar cells in indoor electronics and portable products, thin light-weight flexible/curvable/conformal cells represent the best choice.[10,15] Thin flexible substrates also enable low-cost fabrication processes, such as roll-to-roll (R2R) manufacturing. However, most flexible substrates undergo irreversible degradation at temperatures higher than 150°C,[16] thus imposing a limitation in the choice of materials and architectures for high-performance PSCs, where many of the metal oxide transport and scaffold layers typically require high-temperature treatments. Nevertheless, flexible PSCs have been investigated and developed by using low-temperature fabrication processes on flexible polymeric films, like polyethylene terephthalate (PET) and polyethylene naphthalate (PEN), and also on unconventional substrates, such as paper[17] and other cellulose derivatives;[18] in particular, the highest PCEs reported to date have been 18.4% (at STC)[19] and 13.3% (under low-light indoor LED illumination)[20] for PSCs fabricated on flexible PET films. Especially when analyzing the historic performances under artificial indoor illumination, the efficiencies are over a factor of two lower than their counterparts fabricated on rigid glass substrates. This large gap related to performance of flexible cells under indoor illumination needs to be closed. For this purpose, we have identified and developed conductive ultra-thin flexible glass (FG) as an excellent alternative to PET because of its compatibility with high-temperature processing (up to 700°C) and because it possesses remarkable barrier properties with water vapor transmission rates lower than 7×10^{-6} g m^{-2} d^{-1},[21] avoiding two of the biggest limitations related to plastic films.

All previous developments on FG were for cells operating under 1 sun. Tavakoli et al.[22] fabricated an evaporated n-i-p PSC with FG/indium-doped tin oxide (ITO)/ZnO/$CH_3NH_3PbI_3$/Spiro-MeOTAD/Au architecture that delivered a PCE of 12.1% over a 0.04 cm^2 area, and even up to 13.1% when applying a polydimethylsiloxane (PDMS) antireflection layer. An ITO-free p-i-n solar cell with FG/modified-PEDOT:PSS/$CH_3NH_3PbI_{3-x}Cl_x$/phenyl-C_{61}-butyric acid methyl ester (PCBM)/Ag architecture delivered a maximum PCE of 4.3%.[23] The implementation of AZO/Au/AZO electrode on FG allowed the fabrication of a PSC with FG/AZO/Au/AZO/c-TiO_2/m-TiO_2/$CH_3NH_3PbI_3$/Spiro-MeOTAD/Au architecture, with a PCE of 9.6%.[24] The highest efficiencies under 1 sun for PSCs fabricated on FG were reported for devices based on IZO electrodes: 18.1% was achieved on a 0.1 cm^2 active area for solar cells with a FG/IZO/SnO_2/$Cs_{0.04}MA_{0.16}FA_{0.80}Pb_{1.04}I_{2.6}Br_{0.48}$/Spiro-MeOTAD/$MoO_x$/Al configuration.[25] Furthermore, R2R fabrication was demonstrated by slot-die deposition of the SnO_2 electron transporting layer and the perovskite absorber[26] on FG/IZO substrates, and a maximum PCE of 14.1% was achieved.

Here, we present flexible perovskite solar cells on ultra-thin flexible glass (FG-PSCs) for highly efficient indoor energy harvesting. First, we optimized ITO coatings on ultra-thin flexible glass via a roll-to-roll sputtering procedure and compared the optical and electrical properties of these substrates with commercially available rigid glass/ITO and flexible PET/ITO. Second, we developed flexible PSCs with two different architectures on the ultra-thin glass transparent electrodes and compared their performance with other flexible solar cells, in particular, those on PET. FG-PSCs delivered a maximum PCE of 14.4% under STC. Notably, breakthrough power outputs were achieved when testing the solar cells under artificial white LED indoor illumination, i.e., almost doubling the previous records for flexible PSCs tested at low lighting levels and at the very top for any flexible indoor photovoltaic technology, with PCEs surpassing 20% and 22% at 200 and 400 lx illuminance, respectively.

Please cite this article in press as: Castro-Hermosa et al., Perovskite Photovoltaics on Roll-To-Roll Coated Ultra-thin Glass as Flexible High-Efficiency Indoor Power Generators, Cell Reports Physical Science (2020), https://doi.org/10.1016/j.xcrp.2020.100045

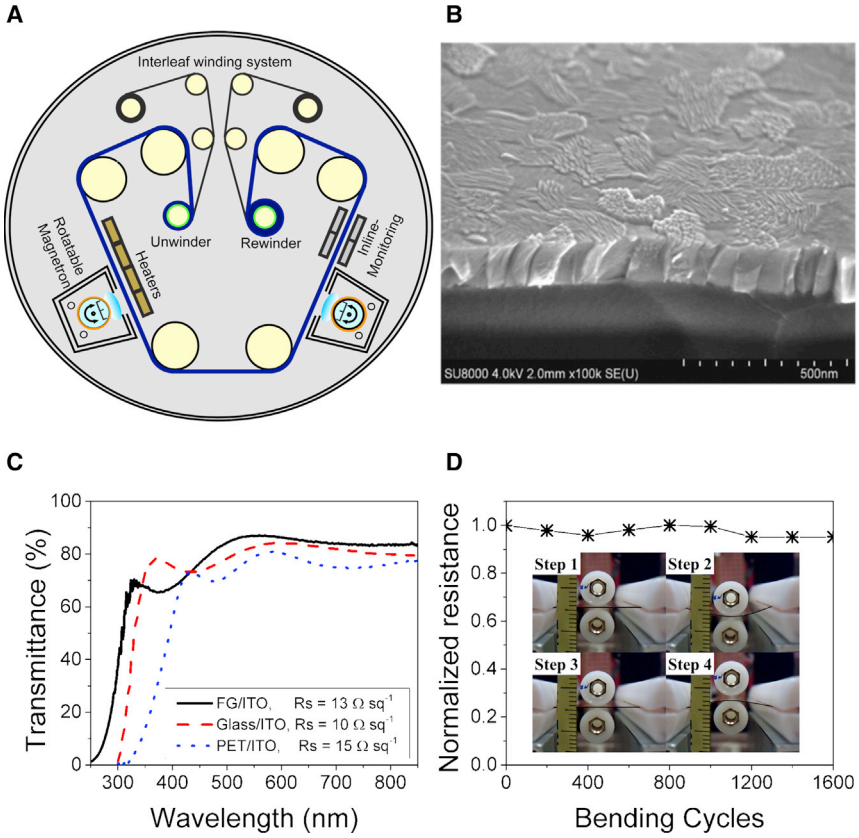

Figure 1. Flexible Glass Substrates Used in the Fabrication of Perovskite Solar Cells

(A) Scheme of the roll-to-roll equipment to deposit the indium tin oxide transparent electrode via rotable magnetron sputtering on a 100-μm-thick glass roll.

(B) SEM image of ITO electrode on top of flexible glass.

(C) Optical transmittance of flexible glass covered with ITO (FG/ITO), rigid glass/ITO, and PET/ITO, with the labels reporting the sheet resistance of each electrode.

(D) Normalized sheet resistance of FG/ITO after 1,600 bending procedures at a bending radius of 20.5 mm. In the inset of (D), the step-by-step process of automated bending test is outlined: first, the sample was placed between the cylindrical force pins (step 1, the ITO layer faced the top cylinder); then, a compressive strength (step 2) was applied followed by an intermediate relaxation state (step 3) and the application of a tensile strength (step 4); and finalized, returning to the initial position (step 1). The yellow scale is in millimeters. Note that, because at each cycle, the substrate is bent inwardly and outwardly 800 times, at the end of the test (D), it has been bent a total of 1,600 times.

RESULTS AND DISCUSSION

Ultrathin Flexible ITO/Glass Substrates

Deposition of ITO via sputtering on a flexible 100-μm-thick glass roll was carried out on a roll-to-roll coating machine with a rotable magnetron and radiation heaters placed between the initial unwinder and final winder elements, with the glass substrate steered through additional six rolls according to the scheme shown in Figure 1A. Compared to plastic films, the development of flexible glass allows the ITO electrode to be deposited at higher substrate temperatures than 140°C–150°C, at which plastic PET films start to deform appreciably.[16] Surpassing this limit and heating substrates in the 160°C–310°C range is essential to obtain a better compromise between optoelectrical properties and morphology of the oxide.[27] For this study, we utilized 190°C for the substrate temperature obtaining 140-nm-thick ITO with very smooth surfaces with a root mean square (RMS) roughness of ~4 nm, which is

Please cite this article in press as: Castro-Hermosa et al., Perovskite Photovoltaics on Roll-To-Roll Coated Ultra-thin Glass as Flexible High-Efficiency Indoor Power Generators, Cell Reports Physical Science (2020), https://doi.org/10.1016/j.xcrp.2020.100045

Table 1. Photovoltaic Parameters of Flexible Perovskite Solar Cells

	E_v (lx)	V_{OC} (V)	J_{SC} (μA cm^{-2})	FF (%)	PCE (%)	MPD (μW cm^{-2})	R_{SH} (kΩ cm^{-2})	R_S (Ω cm^{-2})
FG	200	0.79 ± 0.02 (0.82)	28.5 ± 2.6 (30.7)	65.9 ± 7.8 (72.7)	18.4 ± 2.7 (20.6)	14.9 ± 2.4 (16.7)	270.3	2.5 × 10^3
	400	0.83 ± 0.02 (0.86)	55.5 ± 3.8 (58.8)	69.1 ± 3.3 (73.5)	20.7 ± 1.5 (22.6)	32.0 ± 2.4 (35.0)	340.1	1.2 × 10^3
	1 sun	1.04 ± 0.02 (1.07)	(20.9 ± 1.6) × 10^3 (22.5 × 10^3)	62.4 ± 2.9 (67.8)	13.6 ± 0.8 (14.4)	(13.6 ± 0.8) × 10^3 (14.4 × 10^3)	0.8	9.3
PET	200	0.81 ± 0.01	23.7 ± 2.9	49.6 ± 4.5	12.1 ± 0.5 (12.8)	9.3 ± 0.3 (9.8)	94.8	11.4 × 10^3
	400	0.84 ± 0.01	52.6 ± 7.9	52.6 ± 7.9	12.1 ± 0.7 (13.3)	17.4 ± 1.0 (19.2)	120.0	7.2 × 10^3
	1 sun	1.04 ± 0.01	(20.6 ± 0.3) × 10^3	65.5 ± 1.8	14.1 ± +0.6 (14.8)	14.1 ± +0.6 (14.8 × 10^3)	1.5	9.1

Flexible PSCs with substrate/ITO/SnO_2/m-TiO_2/$CH_3NH_3PbI_3$/Spiro/Au device architecture fabricated on flexible glass (FG) and PET in our laboratories were tested under indoor LED lighting at 200 and 400 lx illuminance and at standard test conditions (1 sun; AM1.5G; 25°C). The average values were calculated on 4 cells for indoor measurements and on 7 samples for measurements at STC; the maximum value is reported in brackets. Parameters for cells on PET are taken from Dagar et al.[20] E_v, illuminance; FF, fill factor; J_{SC}, short-circuit current density; MPD, maximum power density; PCE, power conversion efficiency; R_S, series resistance; R_{SH}, shunt resistance; V_{OC}, open-circuit voltage.

~20% lower than the commercial PET/ITO we utilized (see scanning electron microscope [SEM] image of the FG/ITO surface in Figure 1B). The morphological qualities, combined with the excellent transparency, sheet resistance, and bendability, presented in the following paragraphs, make FG/ITO a beneficial candidate for conformal and curvable photovoltaics.

Significantly, our FG/ITO showed superior optical properties compared to both commercial ITO-coated glass and PET-based conducting substrates (see Table S1 and Figure 1C), with an average transmittance T_{AVE} (measured in the range 350–850 nm) of 81.2%, which was ~2% and ~13% greater (in relative terms) compared to glass/ITO and PET/ITO, respectively, while maintaining a suitable intermediate sheet resistance of 13 Ω/square, between that of rigid glass/ITO (ρ_s = 10 Ω/square) and that of the flexible PET/ITO film (ρ_s = 15 Ω/square). To demonstrate the potential for application in flexible photovoltaics, the electrical resistance of FG/ITO was evaluated over an automated bending test carried out curving the substrate at a radius of 20.5 mm (see inset of Figure 1D) repeatedly. The sheet resistance remained constant, showing a variation of 5% compared to its initial value, which is within the experimental error of our measuring setup, after full 800 bending cycles, corresponding to actual 1,600 bending procedures to put into effect both compressive and tensile stress (see Experimental Procedures), which are known to affect ITO differently,[16] thus proving excellent bendability of our electrodes at this radius of curvature (Figure 1D).

Flexible Perovskite Cells on Ultra-thin Glass under Standard Test Conditions

We developed flexible PSCs on FG/ITO with both planar (FG/ITO/SnO_2/$CH_3NH_3PbI_3$/Spiro/Au) and mesoscopic (FG/ITO/SnO_2/m-TiO_2/$CH_3NH_3PbI_3$/Spiro/Au) n-i-p structures, the difference being the incorporation of an ~150-nm-thick, low-temperature, UV-irradiated mesoporous TiO_2 scaffold. Even though the flexible cells had a slightly lower open circuit voltage (V_{OC}), likely due to an increase in the thickness of the device,[28] the latter outperformed planar devices, delivering a PCE_{AVE} of 13.6% (PCE_{MAX} = 14.4%), compared to PCE_{AVE} = 11.9% (PCE_{MAX} = 13.4%) for planar cells (see Table 1 and Figure 2A). On the contrary, for glass-based devices on commercial thick rigid glass substrates (see Table S2), the average PCE was slightly higher for the planar structure

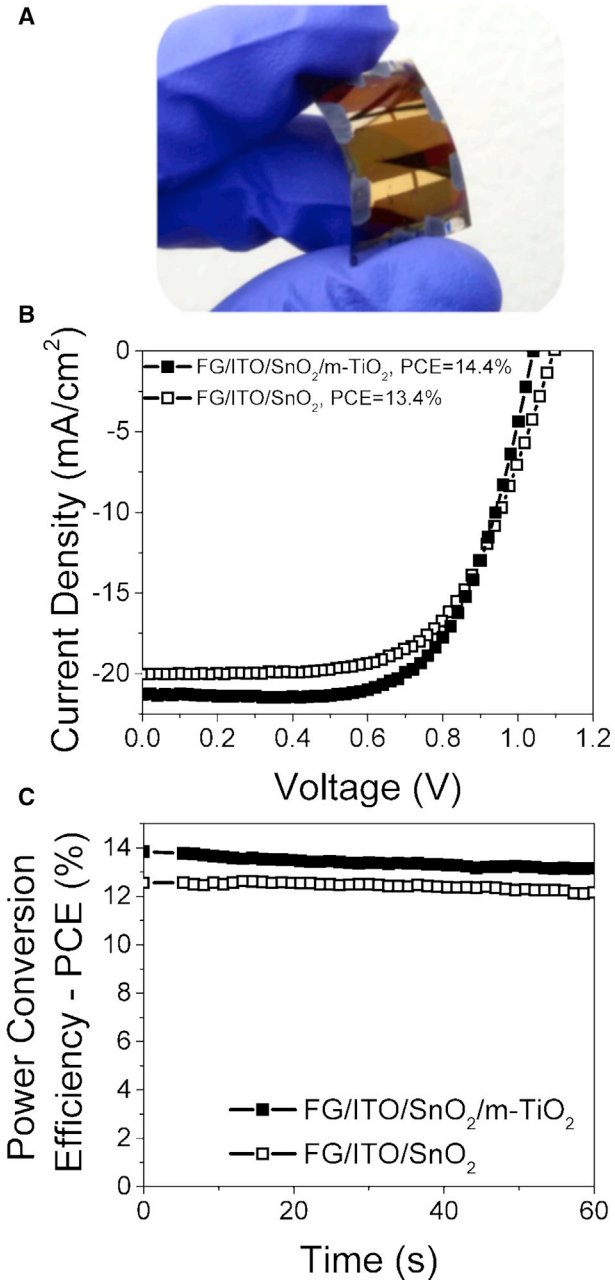

Figure 2. Performance of Planar and Mesoscopic Flexible Perovskite Solar Cells Fabricated on Flexible Glass (FG-PSCs) under Standard Test Conditions

(A) Photograph of a curved FG-PSC.

(B) J-V curves of the best FG-PSCs with device architecture FG/ITO/SnO_2/$CH_3NH_3PbI_3$/spiro-MeOTAD/Au (planar; open squared data points) and FG/ITO/SnO_2/m-TiO_2/$CH_3NH_3PbI_3$/Spiro-MeOTAD/Au (meso; solid squared data points).

(C) Maximum power point tracking (MPPT) of planar and mesoscopic devices fabricated on FG.

Measurements were carried out under standard test conditions (STCs) (1,000 W m^{-2}; AM1.5G; 25°C).

(PCE = 14.5%) compared to the architecture incorporating the TiO_2 scaffold (PCE = 13.5%). Whereas high efficiencies in rigid glass substrate cells can be achieved with planar architectures, especially when optimizing the electron transporting layer,[6] these results show that devices on FG follow a more similar trend to those on ITO/

Please cite this article in press as: Castro-Hermosa et al., Perovskite Photovoltaics on Roll-To-Roll Coated Ultra-thin Glass as Flexible High-Efficiency Indoor Power Generators, Cell Reports Physical Science (2020), https://doi.org/10.1016/j.xcrp.2020.100045

PET regarding the introduction of a scaffold.[20] In fact, the mesoporous TiO_2 is here seen to improve the efficiency (by 14% in relative terms) while reducing hysteresis (hysteresis index HI = 1-PCE_{FOR}/PCE_{REV} reduced from 19% to 6%) due to better wettability of the precursor solutions, perovskite growth compared to growth directly on the compact layer,[29,30] and electron extraction.[20] We carried out quasi-steady-state measurements of the maximum power point (MPPT) under continuous illumination (see Figure 2B). Mesoporous devices presented a stabilized PCE of 13.1%, while planar ones showed a PCE of 12.2% after 60 s of measurement; both values are between the PCE measured in the forward and reverse scans (see Figure S2 and Table S2). External quantum efficiency (EQE) measurements (Figure 3C) were used to calculate the integrated J_{SC} from the AM1.5G photon flux, which was found to be within 10% of the J_{SC} measured under the solar simulator for both cell architectures.

Flexible Perovskite Cells on Ultra-thin Glass under Indoor Illumination

Under artificial indoor LED illumination, mesoscopic cells presented outstanding performances at 200 and 400 lx, surpassing any type of flexible PV technology measured under the same conditions so far. In fact, at 200 lx, the best mesoscopic device presented a PCE of 20.6%; a maximum power density (MPD) of 16.7 μW cm^{-2}; and V_{OC} = 0.82 V, J_{SC} = 30.2 μA cm^{-2}, and FF = 67.2%. When the illuminance was increased up to 400 lx, the same device delivered a PCE of 22.6%; an MPD of 35.0 μW cm^{-2}; and V_{OC} = 0.86 V, J_{SC} = 58.8 μA cm^{-2}, and FF = 68.8% (see Figure 3). These values not only represent a sizeable jump compared to the same cells measured at STC but also represent an order of magnitude improvement in power conversion efficiency compared to planar FG-PSCs (see Figure 4), for which maximum PCEs were 2.3% and 2.8% at 200 and 400 lx, respectively (a dramatic drop from their values at STC). The J_{SC} values measured from the current density vs voltage (J-V) scan were within 16% and 13% of the value of the integrated J_{SC} calculated from the EQE curve and irradiance values at 200 lx and 400 lx and thus within the experimental error of our indoor measurement system (Figure 3C).[31]

We found that carrier recombination was greatly reduced in the mesoscopic structure, as clearly evident from the analysis of the dark currents in Figure 5A. The J_{ON}/J_{OFF} ratios (ratio between the dark current densities at −1 V and 1.5 V) increased by one order of magnitude for the mesoscopic architecture compared to the planar one, mainly by greatly reducing recombination currents. The ratio is in fact of the order of magnitude of 10^4, which, combined with low recombination currents,[6,32,33] represents a figure of merit value, reaching which, cells deliver noteworthy performance under low-light indoor illumination.[30] This is supported by the analysis of the V_{OC} decay (OCVD) and of the photoluminescence (PL) presented in Figures 5B and 5C. The V_{OC} decay of mesoscopic devices is much slower compared to planar cells, showing one order of magnitude improvement in electron lifetime (τ). Recombination was also investigated by measuring the PL emission spectra of samples composed of FG/ETL (electron transporting layer) (i.e., SnO_2 or SnO_2/m-TiO_2)/$CH_3NH_3PbI_3$. The inclusion of a mesoporous scaffold reduces the intensity of the PL peak, confirming a faster collection of charges and reduced recombination of carriers. We also observed a slight red shift compared to planar samples: this could indicate an enhancement in the crystallinity of the perovskite[24,25,34] that has a direct impact in the band gap; the band gap extracted from the maximum peak of PL is 1.57 eV in the case of mesoporous samples, and 1.60 eV for planar samples. In conclusion, the introduction of a TiO_2 mesoporous layer leads to an improvement in the electron extraction and a reduction of the perovskite band gap, which in turn decreases the V_{OC} of mesoscopic FG-PSCs by 3%. This improvement in performance with addition of a mesoscopic layer can be explained by improved growth of

Please cite this article in press as: Castro-Hermosa et al., Perovskite Photovoltaics on Roll-To-Roll Coated Ultra-thin Glass as Flexible High-Efficiency Indoor Power Generators, Cell Reports Physical Science (2020), https://doi.org/10.1016/j.xcrp.2020.100045

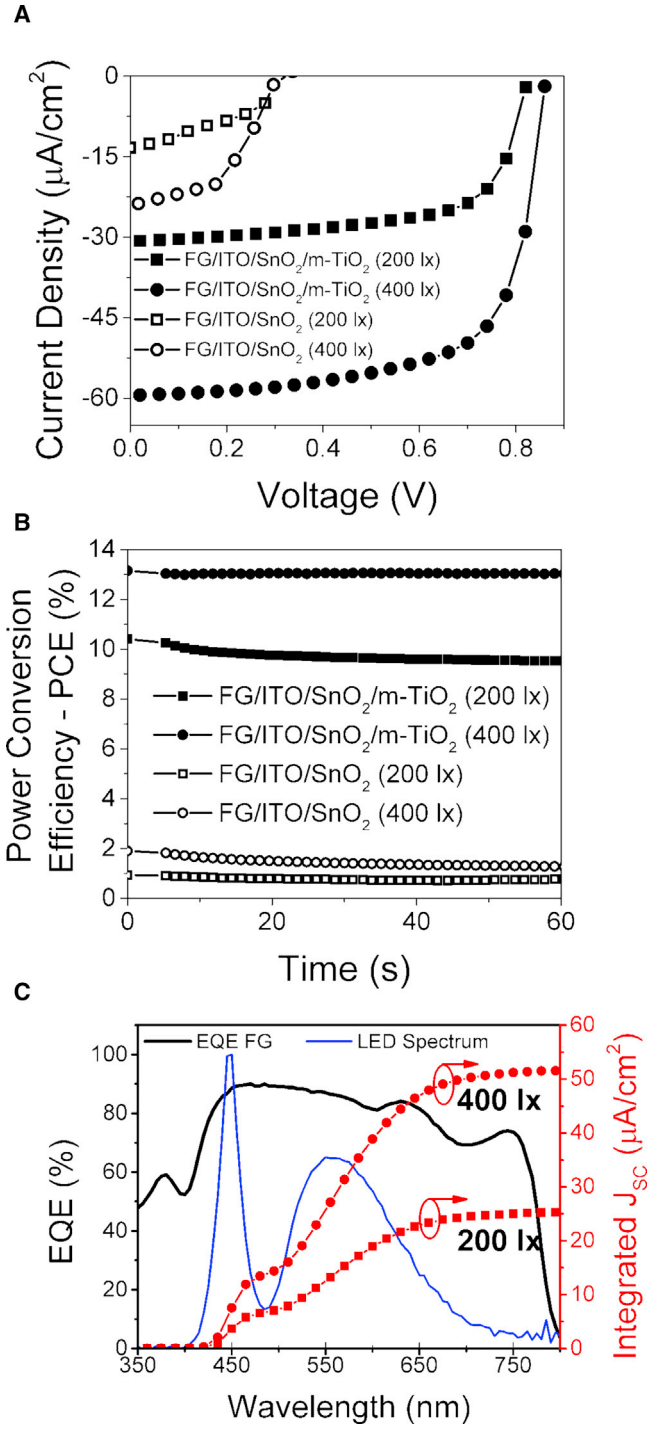

Figure 3. Indoor Performance of PSCs on FG Measured under 200 lx and 400 lx LED Illumination

(A and B) J-V curves (A) and maximum power point tracking (MPPT) (B) of planar (open data points) and mesoscopic (solid data points) FG-PSCs under 200 lx (squared data points) and 400 lx (circular data points) LED illumination (OSRAM P25 white light).

(C) External quantum efficiency (EQE) (continuous black line) and integrated J_{SC} of mesoscopic FG-PSCs under 200 lx (squared data points) and 400 lx (circular data points) illumination; normalized spectrum of the LED lamp (arbitrary units) is reported (continuous blue line).

Please cite this article in press as: Castro-Hermosa et al., Perovskite Photovoltaics on Roll-To-Roll Coated Ultra-thin Glass as Flexible High-Efficiency Indoor Power Generators, Cell Reports Physical Science (2020), https://doi.org/10.1016/j.xcrp.2020.100045

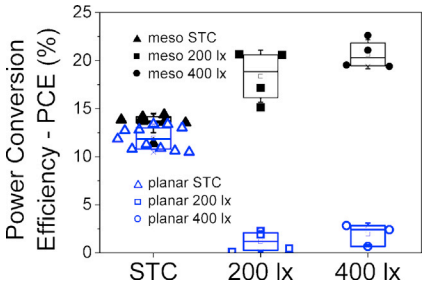

Figure 4. Performance of Planar and Mesoscopic FG-PSCs in Indoor and Simulated Outdoor Conditions

Statistics of the power conversion efficiency (PCE) of planar (blue symbols) and mesoscopic (black symbols) perovskite solar cells on flexible glass tested at STC (1 sun; AM1.5G; 25°C) and under 200 and 400 lx LED illumination. The box represents the 25th and 75th percentiles, and the middle line and the whiskers represent the mean median and the 5th and 95th percentiles, respectively.

the perovskite absorber, which leads to better connected grains compared to that grown directly over the compact layer.[29,30] Better crystallinity can also be inferred by the red shift in the photoluminescence peak (Figure 5C).[34] Reduced hysteresis in the J-V curves signals faster charge separation and electron injection into the electron transporting layer, which can be enhanced with the high-surface-area nanocrystalline TiO_2 and a more intimate interfacial connection between ETL and perovskite semiconductor.[35] Behind this effect can be the wetting of the perovskite precursor over the different ETLs. In fact, contact angle measurements (Figure 6) show that the angle is 47° for the perovskite precursor solution (PbI_2 and CH_3NH_3I dissolved in DMF:DMSO 9:1 v:v) over the SnO_2 compact layer (84° for water), whereas, when measured over the SnO_2/meso-TiO_2 scaffold, the angle approaches 0° for both water and precursor, i.e., a much better wetting of the perovskite at the interface with the ETL. Figure 6 also shows that the contact angle of water over the FG/ITO surface (60°) is intermediate between that of good wetting rigid glass/ITO surface (29°) and the poorly wetting PET/ITO surface (93°), also explaining the differences between fabricating a solar cell on the three different types of substrates.

We investigated the shelf-life stability over 260 days of un-encapsulated FG-PSCs both in the planar and mesoscopic architectures measured at illuminance levels of 200 lx, 400 lx, 1,000 lx, and at STC (see Figure S3). The PSCs retained 80% of their initial PCE for more than 100 days. Following this period, a more rapid drop in performance occurred. It is interesting to note that degradation rates were more rapid when the cells were measured under low light levels compared to under 1 sun. This is not surprising because we have noted already that, to reach high efficiencies under low levels of irradiation, the quality of the transporting and perovskite layers needs to be higher.[30,33] Thus, any degradation will have a greater impact when cells are operated at lower light levels. Differential degradation under 1 sun compared to indoor illumination has previously also been noticed in DSSC technology.[31] A future study must consider encapsulation of the solar cells, which will greatly improve stability compared to un-encapsulated devices. We note that glass, even in its flexible form, is an exceptional glass barrier.[36,37]

Perovskite Cells on Ultra-thin Glass versus Those on PET and Other Technologies under Indoor Illumination

Our results showing efficiencies of over 20%–22% at 200–400 lx for flexible PSCs represent a real breakthrough in performance: in fact, the previous reported highs

Please cite this article in press as: Castro-Hermosa et al., Perovskite Photovoltaics on Roll-To-Roll Coated Ultra-thin Glass as Flexible High-Efficiency Indoor Power Generators, Cell Reports Physical Science (2020), https://doi.org/10.1016/j.xcrp.2020.100045

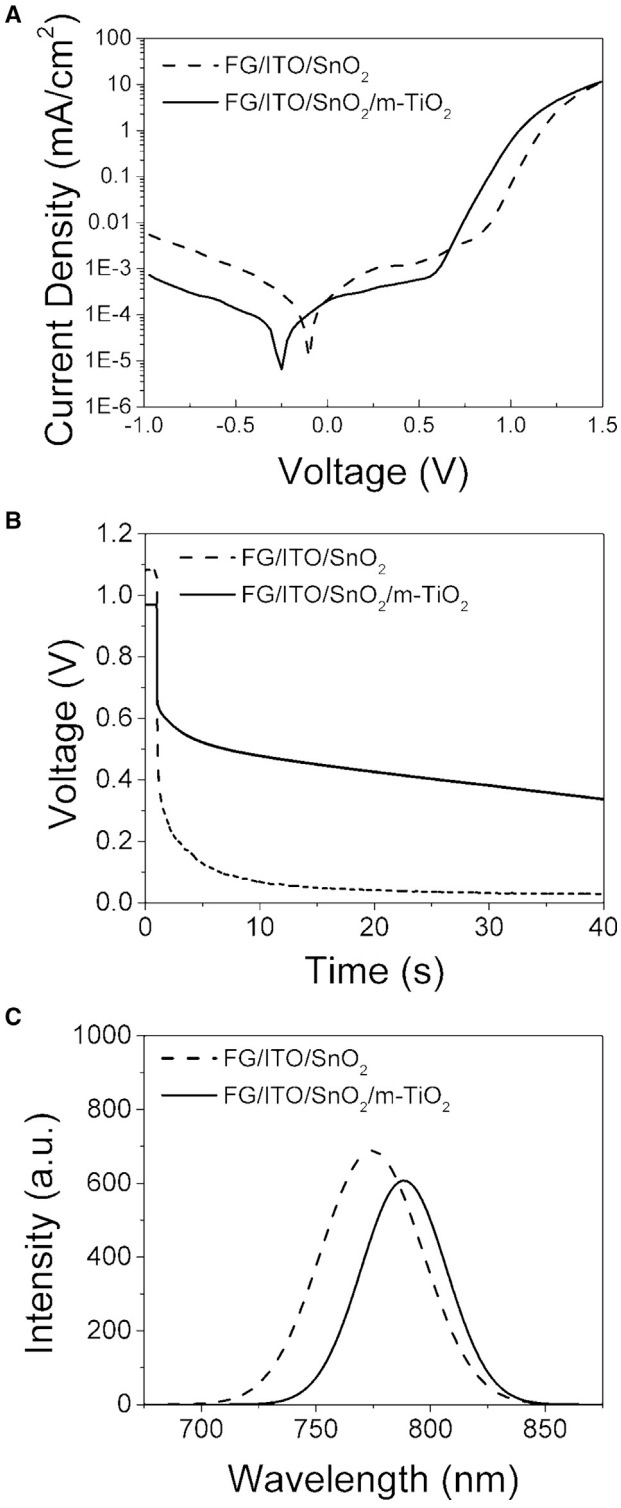

Figure 5. Characterization of PSC on Flexible Glass

(A–C) J-V characteristics in the dark (A) and open-circuit voltage decay (OCVD) (B) of planar (dashed line) and mesoscopic (continuous line) FG-PSCs with FG/ITO/ETL/$CH_3NH_3PbI_3$/spiro-OMeTAD/Au architecture; (C) photoluminescence spectra of FG/ITO/ETL/$CH_3NH_3PbI_3$ stacks (with ETL = SnO_2 in case of the planar stack and SnO_2/m-TiO_2 for the mesoscopic architecture).

Please cite this article in press as: Castro-Hermosa et al., Perovskite Photovoltaics on Roll-To-Roll Coated Ultra-thin Glass as Flexible High-Efficiency Indoor Power Generators, Cell Reports Physical Science (2020), https://doi.org/10.1016/j.xcrp.2020.100045

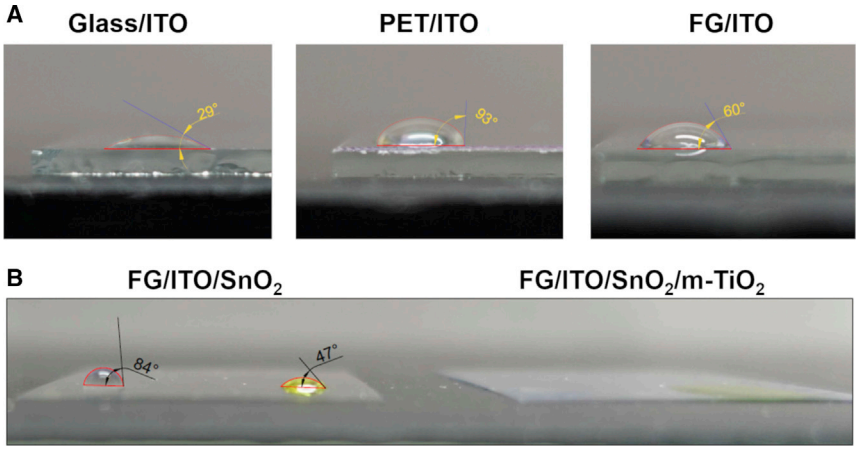

Figure 6. Contact Angle Measurements on ITO Coated on Different Rigid and Flexible Substrates
(A) Contact angle test of water on glass/ITO, PET/ITO, and FG/ITO substrates.
(B) Contact angle test performed with water (transparent drop) and perovskite precursor solution, i.e., PbI_2 and CH_3NH_3I in DMF:DMSO 1:9 v:v (yellow drop), on FG/ITO/SnO_2 (planar) and FG/ITO/SnO_2/mesoporous TiO_2 (mesoporous) samples.

for flexible perovskite photovoltaic cells were those reported by Dagar et al.[20] on PET, where best PCEs were in the same lux range. Our results (see Table 1) represent a jump of between 73% and 90% in MPDs and PCEs. This remarkable upsurge is partially due to a marginally improved photocurrent (by a median of 8%), to which the higher transmittance of the FG/ITO electrode contributes (see Figure 1C), especially in the 350–500 nm range compared to mesoscopic devices on PET (see Dagar et al.[20] for the EQE spectrum of PET-PSCs). Noticeably, Figure 3C shows that the EQE is always above 80% in the 425–660 nm range, at which the LED spectrum is above 20% of its peak, demonstrating that the spectrum of perovskite solar cells covers very well that of the most common source of indoor lighting, i.e., white LEDs. More significant is the enhancement in fill factor that increases from 50% to 53% for cells on PET to 64% to 68% on ultrathin flexible glass and can be ascribed to an improved sheet resistance of the ITO (13 versus 15 Ω/square), the better interface between the layers fabricated on FG, the lower series and higher shunt resistances of FG compared to PET, and the different wettability of the perovskite precursor on FG/ITO and on PET/ITO. In fact, dark currents of FG cells were very low (~0.1 $\mu A\ cm^{-2}$ at −0.5 V), about an order of magnitude lower than those of PET cells.[20] Also, in the 200–400 lx range, the series resistance of devices on FG (2.5 $k\Omega\ cm^2$) was around 80% lower in relative terms compared to those measured in PET cells, whereas the shunt resistance increased by a factor of three (see Table 1), confirming not only a better quality of the ITO deposited on FG but also of the cells' layers and interfaces.

Even at steady state, FG-PSCs maintain the same enhancement in power output (i.e., by 51%–63% in relative terms). In fact, the steady-state PCEs (MPDs) versus time (60 s) for PSCs on ultra-thin glass were 13.0% (20.2 $\mu W\ cm^{-2}$) at 400 lx and 9.5% (7.7 $\mu W\ cm^{-2}$) at 200 lx, whereas these were 8.6% (12.4 $\mu W\ cm^{-2}$) at 400 lx and 6.7% (5.1 $\mu W\ cm^{-2}$) at 200 lx for cells on PET.[20] Hysteresis indices of FG cells were 53% and 47% at 200 and 400 lx (see Figure S4). Hysteresis indices and steady-state values can be improved in the future by developing more effective ETLs even on FG, as recently demonstrated by our group,[6] where by covering the ETL with another insulating high-band-gap oxide, maximum PCEs of 27% and MPD of 42 $\mu W\ cm^{-2}$ (400 lx;

Table 2. Area of Perovskite Solar Cells on Ultra-thin Flexible Glass Required to Power Low-Consumption Sensors for the Internet of Things under 200, 400, and 1,000 lx LED Illumination

Electronic Device	Energy Consumption	Area of FG-PSCs Required		
		200 lx	400 lx	1,000 lx
		PCE = 20.6%	PCE = 22.6%	PCE = ~21%
		MPD = 16.7 μW/cm^2	MPD = 35.0 μW/cm^2	MPD = 78.5 μW/cm^2
RFID	5–15 μW	0.3–0.9 cm^2	0.1–0.4 cm^2	0.1–0.2 cm^2
LoRA backscatter	10–20 μW	0.6–1.2 cm^2	0.3–0.6 cm^2	0.1–0.3 cm^2
Passive Wi-Fi	40–70 μW	2.4–4.2 cm^2	1.1–2.0 cm^2	0.5–0.9 cm^2
Sensors/remotes	100 μW	5.9 cm^2	2.8 cm^2	1.3 cm^2
Still cameras	1.3 mW	77.8 cm^2	36.9 cm^2	16.5 cm^2

Estimates on energy consumption of low-power electronic devices were taken from references[31,38–40], with that of the still camera assuming a 10 s cycle per operation.

LED illumination) were obtained on rigid glass substrates with very low HI factors and steady-state PCEs approaching those measured during the J-V scans.

Such high efficiencies of PV cells on ultra-thin glass opens up the potential for these devices to be integrated in portable devices, wireless sensor nodes, and low-power consumer products working in indoor environments; these types of new devices, being ultra-light, ultra-thin, and flexible, can be curved to be seamlessly integrated in a vast number of surfaces. The remarkable potential of flexible FG-PSCs as indoor energy harvesters is clear if one considers their outstanding efficiencies at low lighting levels. Our flexible cells generate power densities of 16.7 and 35.0 μW/cm^2 under 200 and 400 lx LED illumination. Even higher power outputs can be achieved when increasing the intensity of the light source (see Figure S5), with our mesoscopic devices delivering power outputs of 78.5 μW cm^{-2} under 1,000 lx lighting (V_{OC} = 0.84 V, J_{SC} = 129.0 μA cm^{-2}, FF = 72.8%, and estimated PCE ~21%). Noteworthy, a maximum V_{OC} between 0.82 and 0.86 V in the 200–1,000 lx was obtained for FG-PSCs with low standard deviations (see Table 1). Achieving a high and stable voltage and good reproducibility is fundamental for integration of indoor PV in electronic systems and wireless devices, as it reduces the number of cells required for series connection into a module.[38] The power outputs obtained for our optimized flexible PSCs are compatible with the operation of low-consumption consumer electronics (e.g., wristwatches, calculators, and still cameras)[31,39] and wireless sensors, such as radio-frequency identifier (RFID), low-range (LoRa) backscatter, and passive WiFi,[38,40] which require a power in the 5 μW–1 mW range. FG-PSC with area from 0.1 to tens of cm^2 would fulfill these requirements in the 200–1,000 lx LED illuminance range (see Table 2).

The choice between PET and flexible glass for indoor applications will depend on (1) performance (currently favoring flexible glass as shown here), (2) flexibility and ruggedness as opposed to just bendability (favoring PET, especially when replacing brittle ITO with alternatives, such as dielectric/thin-metal/dielectric layers),[41] (3) stability (favoring flexible glass that has the same outstanding water vapor transmission rates (WVTR)[36] as that of rigid glass, which is over 4 times lower than that of PET, even when paired with adhesive systems for application over electronic devices),[37] and (4) cost (estimates for industrial-scale production range from 6 to 9 $/m^2 for PET[15] to ~40 $/m^2 for flexible glass; https://www.slideshare.net/StuartRock/

Please cite this article in press as: Castro-Hermosa et al., Perovskite Photovoltaics on Roll-To-Roll Coated Ultra-thin Glass as Flexible High-Efficiency Indoor Power Generators, Cell Reports Physical Science (2020), https://doi.org/10.1016/j.xcrp.2020.100045

Table 3. Specific Power, Area Density, and Thickness of Perovskite Solar Cells Fabricated on Ultra-thin Flexible Glass, PET, and Rigid Glass

	Specific Power (W g^{-1})			Area Density (g/m^2)	Thickness (μm)
	STC	400 lx	200 lx		
FG-PSC	0.58	1.4×10^{-3}	0.7×10^{-3}	251	100
PET-PSC	0.74	0.9×10^{-3}	0.5×10^{-3}	198	125
Glass-PSC	0.07	1.5×10^{-4}	0.7×10^{-4}	2,761	1,100

Specific power was calculated as the power output at STC and under 200 and 400 lux LED illumination over the weight of the solar cell. Values for PET- and glass-based devices are taken from references;[6,20] thickness values refer to the substrate only (~1 μm thickness of the cell was omitted, being the same for all the devices).

willow-glass-technology-strategy-presentation), values which will depend on market volumes and uptake as well as the use or not of additional permeation barriers.

Specific power, calculated as power output over weight of the solar cell, is another feature to consider when selecting the optimal substrate for compact and lightweight PSCs. FG-PSCs show superior specific power than PET-PSCs, especially in indoor conditions by a margin of 40%–50% in relative terms. When comparing the specific power of FG-PSCs compared to rigid glass counterparts, the improvement shoots up to an order of magnitude (see Table 3). Note that, in a final product, the cells would need encapsulating: FG with another FG barrier whereas PET with two laminated multilayer barriers unless the PET substrate is first coated with multilayers (then only one would be required).[37]

Finally, the performance of the cells presented in this work are the highest efficiencies reported up to now for any type of flexible photovoltaic technology tested in indoor conditions, showing their great potential to power indoor electronics of the future (see Table 4). For completeness, we note that, according to previous works regarding large area indoor PSCs,[8,42,43] a loss of around 20% in relative terms can be expected when upscaling from small laboratory cells of less than 1 cm^2 area to modules of around 10 cm^2,[42] which would maintain PCEs of FG-PSCs above the high value of 18%. Noteworthy, all the layers of our PSCs were deposited at low temperature and by solution processing (except for the gold electrode), meaning that roll-to-roll fabrication of devices on FG can not only be implemented for the ITO but also for all other layers in the future in order to lower the fabrication costs, improve the production yield of flexible PSCs, and allow the application of such devices as a first choice as indoor light harvesters for low-power electronics, sensor nodes, and the internet of things. The research and development in this field promises many avenues to explore in the future.

EXPERIMENTAL PROCEDURES

Deposition of ITO Electrodes on Flexible Glass

Our FG substrate consisted in a roll of a 100-μm-thick glass (AF32 from SCHOTT); for deposition of the ITO electrode, the FG roll went through the roll-to-roll coating machine of Figure 1A. (VON ARDENNE). The glass was heated by thermal radiation from the backside while passing through the deposition zone; during deposition, a temperature of 130–310°C can be reached. ITO (In_2O_3/10 wt %SnO_2) was deposited by sputtering from a ceramic target (TOSOH) on a rotatable magnetron (SOLERAS). A DC power of 3 kW was applied for a target of 65 cm length. The substrate moved with a speed of 0.28 m min^{-1}, resulting in the deposition of an ITO layer with approximately 140 nm thickness. Further details can be found elsewhere.[27]

Please cite this article in press as: Castro-Hermosa et al., Perovskite Photovoltaics on Roll-To-Roll Coated Ultra-thin Glass as Flexible High-Efficiency Indoor Power Generators, Cell Reports Physical Science (2020), https://doi.org/10.1016/j.xcrp.2020.100045

Table 4. Best Photovoltaic Performance for Flexible Solar Cells Tested under Indoor Illumination

Technology	Device	Flexibility	Area (cm^2)	Light Source	E_V (lx)	MPD ($\mu W\ cm^{-2}$)	PCE (%)	Ref.
a-Si	a-Si:H	bending radius 2 cm	30.0	FL	300	8.0	8.7	47
III-V	GaAs (Alta Devices)	bending radius <15 cm	50.0	FL	200	13.1	18.6	4
					1,000	74.5	21.0	4
OPV	n-i-p SnO_2/PV2001:PCBM-based device on PET	flexible	0.3	LED	200	9.1	12.9	48
				LED	400	17.9	12.6	48
				LED	1,000	45.4	12.7	48
DSSC	DSSC with optimized electrolyte (CHOSE)	flexible	0.3	CFL	200	7.9	12.4	31
				LED	200	6.6	10.0	31
	AN11-sensitized module	flexible	19.8	CFL	1,000	32.5	9.6	49
				LED	200	5.1	8.1	49
					1,000	30.1	9.5	49
PSC	n-i-p SnO_2/m-TiO_2- based device on PET (CHOSE)	flexible	0.1	LED	200	9.8	12.9	20
					400	19.2	13.3	20
	n-i-p SnO_2/m-TiO_2 -based device on ultra-thin flexible glass (CHOSE)	bending radius 20.5 mm	0.1	LED	200	16.7	20.6	this work
					400	35	22.6	this work

CFL, compact fluorescent light; FL, fluorescent light; LED, light-emitting diode

The roughness of the FG/ITO samples was measured using a Nanite B atomic force microscope (AFM) from Nanosurf.

Fabrication of Perovskite Solar Cells

All solvents and reagents, if not specified, were purchased from Sigma Aldrich and used as received. PSCs were fabricated in an n-i-p configuration, with or without a mesoporous TiO_2 scaffold (FG/ITO/SnO_2/$CH_3NH_3PbI_3$/Spiro-OMeTAD/Au and FG/ITO/SnO_2/TiO_2/$CH_3NH_3PbI_3$/Spiro-OMeTAD/Au). FG/ITO substrates were laser cut and then patterned by wet etching in HBr at 100°C for 10 min and cleaned in ultrasonic bath in soapy water, acetone, and isopropanol consecutively, for 15 min each (the samples were blow dried with dry air between any change of solvent). The SnO_2 compact layer was deposited by spin coating a 0.1 M precursor solution of $SnCl_2$:$2H_2O$ in ethanol (96%). The substrates were subjected to UV irradiation with an estimated power density of 2250 W m^{-2} (Dymax EC 5,000 UV lamp with a metal-halide bulb PN38560 Dymax with no UV-C) for 10 min and blow dried with air (only if necessary, i.e., if visible particles were on the ITO surface). Then, the SnO_2 precursor solution was spin coated in a double-step process in air by dropping 100 μL at 1,500 rpm for 30 s and then 100 μL at 2,500 rpm for 30 s; films were annealed at 150°C for 1 h. In case of mesoscopic devices, the mesoporous layer was deposited by spin coating a diluted TiO_2 paste (18N-RT; Greatcell Solar Ltd.; 1:5 v:v) at 3,000 rpm for 30 s, annealed at 150°C for 15 min, and finally subjected to a UV-sintering process for 1.5 h (with the same UV previously described). The active layer ($CH_3NH_3PbI_3$) was prepared by using a solvent engineering method as reported in Ahn et al.[44] The precursor solution was obtained by dissolving PbI_2 (TCI, 99.99%) and CH_3NH_3I (Greatcell Solar Ltd.) in a 1:1 molar ratio in a solvent mixture composed of dimethylformamide (DMF) (99.8%) and dimethyl sulfoxide (DMSO) (99.5%; 9:1, v:v) to obtain a final concentration of 1.4 M. The film was formed in a two-step, spin-coating process consisting of 1,000 rpm for 10 s, followed by 5,000 rpm for 45 s; 35 s before the end of the process, 0.7 mL of diethyl ether were dropped on the rotating substrate. Perovskite films were annealed at 50°C for 2 min and 100°C for 10 min. All the deposition

Please cite this article in press as: Castro-Hermosa et al., Perovskite Photovoltaics on Roll-To-Roll Coated Ultra-thin Glass as Flexible High-Efficiency Indoor Power Generators, Cell Reports Physical Science (2020), https://doi.org/10.1016/j.xcrp.2020.100045

processes mentioned above were carried out in air atmosphere (relative humidity below 40%). After the perovskite deposition, the samples were transferred to a nitrogen-filled glovebox for the deposition of the hole transporting layer (HTL). The Spiro-OMeTAD (Borun New Material Technology Ltd.) was dissolved in chlorobenzene (99.8%) to obtain a final concertation of 73.5 mg mL^{-1}. 2 h before the deposition, the solution was doped with 26.7 μL mL^{-1} of 4-tert-butylpyridine (TBP), 16.6 μL mL^{-1} of a bis(trifluoromethylsulfonyl)amine lithium salt) (LiTFSI) solution (520 mg/mL in acetonitrile; 99.8%), and 7.2 μL mL^{-1} of FK209 cobalt(III) complex solution (375 mg mL^{-1} in acetonitrile) and spin-coated on the perovskite film at 2,500 rpm for 20 s. The Au back electrode was thermally evaporated at a pressure range of 4–6 × 10^{-6} mbar, using a shadow mask to define an active area of 0.1 cm^2.

Characterization

UV-Vis absorption spectra were recorded using a UV-vis 2550 Spectrophotometer from Shimadzu. The sheet resistance was measured with a four-point probe. Imaging of the ITO surface morphology on FG was carried out with a scanning electron microscope (SEM) Hitachi SU8000. Bending test setup was based on an Arduino UNO electronic card, which controlled a stepper motor with a linear movement of 23 μm per motor step. The FG/ITO substrate was placed between two cylindrical plastic force pins and two plastic supporters (see inset in Figure 1D), with the ITO layer facing the top cylinder. A single bending cycle was constituted by four steps: once the sample was placed in the holder (step 1), a compressive bending procedure (step 2) was applied followed by an intermediate relaxation state (step 3), the application of a tensile bending procedure (step 4), and finally it was returned to the initial position. The J-V characteristics of the solar cells were measured with a Keithley2420 source meter under a calibrated Class A ABET solar simulator (AM1.5G; 1,000 W m^{-2}) at room temperature. For the indoor characterization, a customized home-built setup was employed; details about the setup can be found in our previous works.[31] We used a LED lamp (OSRAM Parathom Classic P25 4W daylight, 250 lm, whose spectrum is shown in supporting information; Figure S1) as light source and changed the distance of the solar cells from the source in order to achieve an illuminance of 200 and 400 lx. Prior to each measurement, the illuminance was measured with a NIST-traceable calibrated Digisense 20250-00 luxmeter. In order to calculate the power conversion efficiency in indoors, the power density impinging on the devices at 200 and 400 lx was measured with an International Light Technologies ILT900 NIST-traceable calibrated spectroradiometer. For all J-V measurements, the scan rate was fixed at 30 mV/s and the cells masked with a black tape to define an active area of 0.1 cm^2. Statistics of the PV parameters of planar and mesoscopic FG-PSCs was calculated on 4 cells from different batches for indoor measurements and on an average of 9 cells from different batches for measurements at STC. The EQE and PL measurements were performed by using a customizable all-in-one measurement platform (Arkeo; Cicci Research s.r.l). The PL was measured using a monochromatic light coupled to a spectrometer with a range between 360 and 1,100 nm and a full width at half maximum (FWHM) equal to 2.4 nm. The EQE measurements were performed using an integrated IPCE (incident photon-to-current conversion efficiency) module. IPCE module has a UV-enhanced silicon photodiode calibrated by NIST and a monochromatic line composed by a xenon lamp (ozone-free) with a tunable range of 300–1,800 nm. The spectral resolution was 5 nm. EQE allowed to calculate the J_{SC} through integration with the irradiance spectra (for both 1 sun AM1.5G solar spectrum and LED indoor spectrum at 200 and 400 lx). Stabilized power conversion efficiency over time was measured at constant bias at the maximum power point voltage. The open circuit voltage decay (OCVD) was measured using a mechanical shutter integrated in the solar simulator and recording the V_{OC} as a function of

time (t > 30 s) with a Metrohm Autolab potentiostat/galvanostat. The electron lifetime (t_n) was calculated using the well-known equation reported in Zaban et al.[45] The stability of un-encapsulated FG-PSCs was studied following the ISOS-1-D protocol.[46] Contact angle measurements were done by slowly dropping water or perovskite precursor solution (PbI_2 and CH_3NH_3I in DMF:DMSO 1:9 v:v) on top of the samples and taking pictures with a high-resolution camera. Angles were measured using Autodesk AutoCAD software.

DATA AND CODE AVAILABILITY

All data associated with the study are included in the paper and the Supplemental Information.

SUPPLEMENTAL INFORMATION

Supplemental Information can be found online at https://doi.org/10.1016/j.xcrp.2020.100045.

ACKNOWLEDGMENTS

We thank Janardan Dagar from Helmholtz-Zentrum Berlin for useful initial discussions on cell designs. Authors from CHOSE acknowledge Departamento del Huila's Scholarship Program no. 677 from Huila, Colombia for funding, the Air Force Office of Scientific Research for funding the international program through grant number FA9550-18-1-0233 (Bio Physics and Natural Materials), the European Union's Horizon 2020 research and innovation programme under grant agreement no. 763989 APOLO, the Italian Space Agency (ASI) project, PEROSKY-Perovskite and other printable materials for energy application in space (no. 2018-1-R.0), the University of Rome Tor Vergata's "Mission: Sustainability" "BiCVision" project, Lazio Region "Gruppi di Ricerca" project no. 85-2017-15373 (SIROH) according to L.R. Lazio 13/08, and the Italian Ministry of University and Research (MIUR) through the PRIN2017 BOOSTER (project no. 2017YXX8AZ) grant for funding. This publication reflects only the authors' views, and the funding agencies are not liable for any use that may be made of the information contained therein.

AUTHOR CONTRIBUTIONS

S.C.-H. and G.L. carried out design and fabrication of the perovskite solar cells and the experiments, including JV characteristics under STC, dark and indoor illumination, external quantum efficiency, optical transmittance, photoluminescence, and voltage decay measurements; analyzed the data; and participated in writing the paper. S.C.-H. developed the bending test setup. M.T., M.F., and J.F. developed the ITO electrodes on ultra-thin flexible glass substrates and provided valuable input at all stages as well as providing SEM images. T.M.B. envisioned and supervised the solar cell experiments, analysis of the data, and writing of the article.

DECLARATION OF INTERESTS

The authors declare no competing interests.

Received: September 18, 2019
Revised: December 30, 2019
Accepted: March 4, 2020
Published: April 29, 2020

REFERENCES

1. National Renewable Enery Laboratory (2019). Best research-cell efficiency chart. https://www.nrel.gov/pv/cell-efficiency.html.
2. Nam, M., Kang, J., Shin, J., Na, J., Park, Y., Cho, J., Kim, B., Lee, H.H., Chang, R., and Ko, D.-H. (2019). Ternary organic blend approaches for high photovoltaic performance in versatile applications. Adv. Energy Mater. *9*, 1901856.
3. Cui, Y., Wang, Y., Bergqvist, J., Yao, H., Xu, Y., Gao, B., Yang, C., Zhang, S., Inganäs, O., Gao, F., et al. (2019). Wide-gap non-fullerene acceptor enabling high-performance organic photovoltaic cells for indoor applications. Nat. Energy *4*, 768–775.
4. Freitag, M., Teuscher, J., Saygili, Y., Zhang, X., Giordano, F., Liska, P., Hua, J., Zakeeruddin, S.M., Moser, J.-E., Grätzel, M., et al. (2017). Dye-sensitized solar cells for efficient power generation under ambient lighting. Nat. Photonics *11*, 372–378.
5. Cao, Y., Liu, Y., Zakeeruddin, S.M., Hagfeldt, A., and Grätzel, M. (2018). Direct contact of selective charge extraction layers enables high-efficiency molecular photovoltaics. Joule *2*, 1108–1117.
6. Dagar, J., Castro-Hermosa, S., Lucarelli, G., Cacialli, F., and Brown, T.M. (2018). Highly efficient perovskite solar cells for light harvesting under indoor illumination via solution processed SnO_2/MgO composite electron transport layers. Nano Energy *49*, 290–299.
7. Chen, C.-Y., Lee, W.-H., Hsiao, S.-Y., Tsai, W.-L., Yang, L., Lin, H.-L., Chou, H.-J., and Lin, H.-W. (2019). Vacuum-deposited perovskite photovoltaics for highly efficient environmental light energy harvesting. J. Mater. Chem. A *7*, 3612–3617.
8. Cheng, R., Chung, C.-C., Zhang, H., Liu, F., Wang, W.-T., Zhou, Z., Wang, S., Djurišić, A.B., and Feng, S.-P. (2019). Tailoring triple-anion perovskite material for indoor light harvesting with restrained halide segregation and record high efficiency beyond 36%. Adv. Energy Mater. *9*, 1901980.
9. Li, M., Zhao, C., Wang, Z.-K., Zhang, C.-C., Lee, H.K.H., Pockett, A., Barbé, J., Tsoi, W.C., Yang, Y.-G., Carnie, M.J., et al. (2018). Interface modification by ionic liquid: a promising candidate for indoor light harvesting and stability improvement of planar perovskite solar cells. Adv. Energy Mater. *8*, 1801509.
10. Reese, M.O., Glynn, S., Kempe, M.D., McGott, D.L., Dabney, M.S., Barnes, T.M., Booth, S., Feldman, D., and Haegel, N.M. (2018). Increasing markets and decreasing package weight for high-specific-power photovoltaics. Nat. Energy *3*, 1002–1012.
11. Razza, S., Castro-Hermosa, S., Di Carlo, A., and Brown, T.M. (2016). Research update: large-area deposition, coating, printing, and processing techniques for the upscaling of perovskite solar cell technology. APL Mater. *4*, 091508.
12. Abbel, R., Galagan, Y., and Groen, P. (2018). Roll-to-roll fabrication of solution processed electronics. Adv. Eng. Mater. *20*, 1701190.
13. Mathews, I., Kantareddy, S.N., Buonassisi, T., and Peters, I.M. (2019). Technology and market perspective for indoor photovoltaic cells. Joule *3*, 1415–1426.
14. Fiorini, P., Doms, I., Van Hoof, C., and Vullers, R. (2008). Micropower energy scavenging. In ESSCIRC 2008 - 34th European Solid-State Circuits Conference (IEEE), pp. 4–9.
15. Di Giacomo, F., Fakharuddin, A., Jose, R., and Brown, T.M. (2016). Progress, challenges and perspectives in flexible perovskite solar cells. Energy Environ. Sci. *9*, 3007–3035.
16. Zardetto, V., Brown, T.M., Reale, A., and Di Carlo, A. (2011). Substrates for flexible electronics: A practical investigation on the electrical, film flexibility, optical, temperature, and solvent resistance properties. J. Polym. Sci. B Polym. Physiol. *49*, 638–648.
17. Castro-Hermosa, S., Dagar, J., Marsella, A., and Brown, T.M. (2017). Perovskite solar cells on paper and the role of substrates and electrodes on performance. IEEE Electron Device Lett. *38*, 1278–1281.
18. Brunetti, F., Operamolla, A., Castro-Hermosa, S., Lucarelli, G., Manca, V., Farinola, G.M., and Brown, T.M. (2019). Printed solar cells and energy storage devices on paper substrates. Adv. Funct. Mater. *29*, 1806798.
19. Feng, J., Zhu, X., Yang, Z., Zhang, X., Niu, J., Wang, Z., Zuo, S., Priya, S., Liu, S.F., and Yang, D. (2018). Record efficiency stable flexible perovskite solar cell using effective additive assistant strategy. Adv. Mater. *30*, e1801418.
20. Dagar, J., Castro-Hermosa, S., Gasbarri, M., Palma, A.L., Cina, L., Matteocci, F., Calabrò, E., Di Carlo, A., and Brown, T.M. (2018). Efficient fully laser-patterned flexible perovskite modules and solar cells based on low-temperature solution-processed SnO_2/mesoporous-TiO_2 electron transport layers. Nano Res. *11*, 2669–2681.
21. Burst, J.M., Rance, W.L., Meysing, D.M., Wolden, C.A., Metzger, W.K., Garner, S.M., Cimo, P., Barnes, T.M., Gessert, T.A., and Reese, M.O. (2014). Performance of transparent conductors on flexible glass and plastic substrates for thin film photovoltaics. 2014 IEEE 40th Photovoltaic Specialist Conference (PVSC) (IEEE), 1589–1592.
22. Tavakoli, M.M., Tsui, K.-H., Zhang, Q., He, J., Yao, Y., Li, D., and Fan, Z. (2015). Highly efficient flexible perovskite solar cells with antireflection and self-cleaning nanostructures. ACS Nano *9*, 10287–10295.
23. Ballipinar, F., Rastogi, A.C., Garner, S.M., and Darling, S.B. (2016). Planar mixed halide perovskite-PCBM solar cells on flexible glass substrates processed at low temperature without ITO. 2016 IEEE 43rd Photovoltaic Specialists Conference (PVSC) (IEEE), 1611–1616.
24. Dang, T.-V., Pammi, S.V.N., Choi, J., and Yoon, S.-G. (2017). Utilization of AZO/Au/AZO multilayer electrodes instead of FTO for perovskite solar cells. Sol. Energy Mater. Sol. Cells *163*, 58–65.
25. Dou, B., Miller, E.M., Christians, J.A., Sanehira, E.M., Klein, T.R., Barnes, F.S., Shaheen, S.E., Garner, S.M., Ghosh, S., Mallick, A., et al. (2017). High-performance flexible perovskite solar cells on ultrathin glass: implications of the TCO. J. Phys. Chem. Lett. *8*, 4960–4966.
26. Dou, B., Whitaker, J.B., Bruening, K., Moore, D.T., Wheeler, L.M., Ryter, J., Breslin, N.J., Berry, J.J., Garner, S.M., Barnes, F.S., et al. (2018). Roll-to-roll printing of perovskite solar cells. ACS Energy Lett. *3*, 2558–2565.
27. Fahland, M., Zywitzki, O., Modes, T., Vondkar, K., Werner, T., Ottermann, C., Berendt, M., and Pollack, G. (2019). Roll-to-roll sputtering of indium tin oxide layers onto ultrathin flexible glass. Thin Solid Films *669*, 56–59.
28. Sha, W.E.I., Ren, X., Chen, L., and Choy, W.C.H. (2015). The efficiency limit of $CH_3NH_3PbI_3$ perovskite solar cells. Appl. Phys. Lett. *106*, 221104.
29. Di Giacomo, F., Zardetto, V., D'Epifanio, A., Pescetelli, S., Matteocci, F., Razza, S., Di Carlo, A., Licoccia, S., Kessels, W.M.M., Creatore, M., et al. (2015). Flexible perovskite photovoltaic modules and solar cells based on atomic layer deposited compact layers and UV-irradiated TiO_2 scaffolds on plastic substrates. Adv. Energy Mater. *5*, 1401808.
30. Lucarelli, G., Di Giacomo, F., Zardetto, V., Creatore, M., and Brown, T.M. (2017). Efficient light harvesting from flexible perovskite solar cells under indoor white light-emitting diode illumination. Nano Res. *10*, 2130–2145.
31. De Rossi, F., Pontecorvo, T., and Brown, T.M. (2015). Characterization of photovoltaic devices for indoor light harvesting and customization of flexible dye solar cells to deliver superior efficiency under artificial lighting. Appl. Energy *156*, 413–422.
32. Lechêne, B.P., Cowell, M., Pierre, A., Evans, J.W., Wright, P.K., and Arias, A.C. (2016). Organic solar cells and fully printed super-capacitors optimized for indoor light energy harvesting. Nano Energy *26*, 631–640.
33. Di Giacomo, F., Zardetto, V., Lucarelli, G., Cinà, L., Di Carlo, A., Creatore, M., and Brown, T.M. (2016). Mesoporous perovskite solar cells and the role of nanoscale compact layers for remarkable all-round high efficiency under both indoor and outdoor illumination. Nano Energy *30*, 460–469.
34. Zhao, P., Yin, W., Kim, M., Han, M., Song, Y.J., Ahn, T.K., and Jung, H.S. (2017). Improved carriers injection capacity in perovskite solar cells by introducing A-site interstitial defects. J. Mater. Chem. A *5*, 7905–7911.
35. Kim, H.S., and Park, N.G. (2014). Parameters affecting I-V hysteresis of CH3NH3PbI3 perovskite solar cells: Effects of perovskite crystal size and mesoporous TiO2 layer. J. Phys. Chem. Lett. *5*, 2927–2934.
36. Reese, M.O., and Barnes, T.M. (2017). Flexible glass in thin film photovoltaics. In Flexible Glass, S.M. Garner, ed. (John Wiley & Sons), pp. 211–246.
37. Castro-Hermosa, S., Top, M., Dagar, J., Fahlteich, J., and Brown, T.M. (2019).

Quantifying performance of permeation barrier—encapsulation systems for flexible and glass-based electronics and their application to perovskite solar cells. Adv. Electron. Mater. *5*, 1800978.

38. Mathews, I., Kantareddy, S.N.R., Sun, S., Layurova, M., Thapa, J., Correa-Baena, J.-P., Bhattacharyya, R., Buonassisi, T., Sarma, S., and Peters, I.M. (2019). Self-powered sensors enabled by wide-bandgap perovskite indoor photovoltaic cells. Adv. Funct. Mater. *29*, 1904072.

39. Kim, S., Jahandar, M., Jeong, J.H., and Lim, D.C. (2019). Recent progress in solar cell technology for low-light indoor applications. Curr. Altern. Energy *3*, 3–17.

40. Talla, V., Hessar, M., Kellogg, B., Najafi, A., Smith, J.R., and Gollakota, S. (2017). LoRa backscatter: enabling the vision of ubiquitous connectivity. Proc. ACM Interact. Mob. Wearable Ubiquitous Technol. *1*, 1–24.

41. Lucarelli, G., and Brown, T.M. (2019). Development of highly bendable transparent window electrodes based on MoO_x, SnO_2, and Au dielectric/metal/dielectric stacks: application to indium tin oxide (ITO)-free perovskite solar cells. Front. Mater. *6*, 1–17.

42. Lee, H.K.H., Barbé, J., Meroni, S.M.P., Du, T., Lin, C.-T., Pockett, A., Troughton, J., Jain, S.M., De Rossi, F., Baker, J., et al. (2019). Outstanding indoor performance of perovskite photovoltaic cells - effect of device architectures and interlayers. Sol. RRL *3*, 1800207.

43. De Rossi, F., Baker, J.A., Beynon, D., Hooper, K.E.A., Meroni, S.M.P., Williams, D., Wei, Z., Yasin, A., Charbonneau, C., Jewell, E.H., et al. (2018). All printable perovskite solar modules with 198 cm^2 active area and over 6% efficiency. Adv. Mater. Technol. *3*, 1800156.

44. Ahn, N., Son, D.-Y.Y., Jang, I.-H.H., Kang, S.M., Choi, M., and Park, N.-G.G. (2015). Highly reproducible perovskite solar cells with average efficiency of 18.3% and best efficiency of 19.7% fabricated via Lewis base adduct of lead(II) iodide. J. Am. Chem. Soc. *137*, 8696–8699.

45. Zaban, A., Greenshtein, M., and Bisquert, J. (2003). Determination of the electron lifetime in nanocrystalline dye solar cells by open-circuit voltage decay measurements. ChemPhysChem *4*, 859–864.

46. Reese, M.O., Gevorgyan, S.A., Jørgensen, M., Bundgaard, E., Kurtz, S.R., Ginley, D.S., Olson, D.C., Lloyd, M.T., Morvillo, P., Katz, E.A., et al. (2011). Consensus stability testing protocols for organic photovoltaic materials and devices. Sol. Energy Mater. Sol. Cells *95*, 1253–1267.

47. Foti, M., Tringali, C., Battaglia, A., Sparta, N., Lombardo, S., and Gerardi, C. (2014). Efficient flexible thin film silicon module on plastics for indoor energy harvesting. Sol. Energy Mater. Sol. Cells *130*, 490–494.

48. Ylikunnari, M., Välimäki, M., Väisänen, K.-L., Kraft, T.M., Sliz, R., Corso, G., Po, R., Barbieri, R., Carbonera, C., Gorni, G., et al. (2020). Flexible OPV modules for highly efficient indoor applications. Flex. Print. Electron. *5*, 14008.

49. Tsai, M.-C., Wang, C.-L., Chang, C.-W., Hsu, C.-W., Hsiao, Y.-H., Liu, C.-L., Wang, C.-C., Lin, S.-Y., and Lin, C.-Y. (2018). A large, ultra-black, efficient and cost-effective dye-sensitized solar module approaching 12% overall efficiency under 1000 lux indoor light. J. Mater. Chem. A *6*, 1995–2003.